Journal Pre-proof

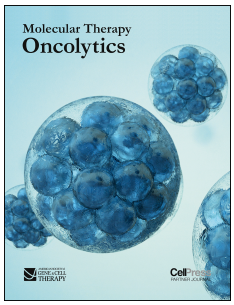

The PERK inhibitor GSK2606414 enhances reovirus infection in head and neck squamous cell carcinoma via an ATF4-dependent mechanism

M. McLaughlin, M. Pedersen, V. Roulstone, K.F. Bergerhoff, H.G. Smith, H. Whittock, J. Kyula, M.T. Dillon, H. Pandha, R. Vile, A. Melcher, K.J. Harrington

PII: S2372-7705(20)30007-3

DOI: https://doi.org/10.1016/j.omto.2020.01.001

Reference: OMTO 172

To appear in: *Molecular Therapy: Oncolytics*

Received Date: 25 June 2019

Accepted Date: 2 January 2020

Please cite this article as: McLaughlin M, Pedersen M, Roulstone V, Bergerhoff K, Smith H, Whittock H, Kyula J, Dillon M, Pandha H, Vile R, Melcher A, Harrington K, The PERK inhibitor GSK2606414 enhances reovirus infection in head and neck squamous cell carcinoma via an ATF4-dependent mechanism, *Molecular Therapy: Oncolytics* (2020), doi: https://doi.org/10.1016/j.omto.2020.01.001.

The PERK inhibitor GSK2606414 enhances reovirus infection in head and neck squamous cell carcinoma via an ATF4-dependent mechanism

McLaughlin M[1], Pedersen M[1], Roulstone V[1], Bergerhoff KF[1], Smith HG[1], Whittock H[1], Kyula J[1], Dillon MT[1], Pandha H[2], Vile R[3], Melcher A[1], Harrington KJ[1]

1 The Institute of Cancer Research, London, UK
2 University of Surrey, Guildford, UK
3 Mayo Clinic, Rochester MN, USA

Corresponding author
Martin McLaughlin: martin.mclaughlin@icr.ac.uk

Keywords: Reovirus type 3 Dearing, reolysin, pelareorep, PERK, unfolded protein response, integrated stress response, ER stress, oncolytic virus, ATF4

Short Title: GSK2606414 plus Reovirus in HNSCC

Abstract

Reovirus type 3 Dearing (reovirus) is a tumour-selective oncolytic virus currently under evaluation in clinical trials. Here, we report that the therapeutic efficacy of reovirus in head and neck squamous cell cancer can be enhanced by targeting the unfolded protein response (UPR) kinase, PERK. PERK inhibition by GSK2606414 increased reovirus efficacy in both 2D and 3D models *in vitro*, while perturbing the normal host cell response to reovirus-induced ER stress. UPR reporter constructs were used for live cell 3D spheroid imaging. Profiling of eIF2a-ATF4, IRE1a-XBP1 and ATF6 pathway activity revealed a context-dependent increase in eIF2a-ATF4 signaling due to GSK2606414. GSK2606414 blocked eIF2a-ATF4 signaling due to the canonical ER stress agent thapsigargin. In the context of reovirus infection, GSK2606414 induced eIF2a-ATF4 signaling. Knockdown of eIF2a kinases PERK, GCN2 and PKR revealed eIF2a-ATF4 reporter activity was dependent on either PERK or GCN2. Knockdown of ATF4 abrogated the GSK2606414 induced increase in reovirus protein levels, confirming eIF2a-ATF signaling as key to the observed phenotype. Our work identifies a novel approach to enhance the efficacy and replication of reovirus in a therapeutic setting.

Introduction

Reovirus type 3 Dearing (abbreviated hereafter as reovirus) is an immuno-oncolytic virus under active clinical development. It has been granted orphan drug status by the FDA for malignant glioma. It is a segmented, double-stranded RNA virus with 10 genome segments. Viral proteins provide self-sufficiency in relation to cellular entry via JAM1 and β1-integrins, endosomal escape allowing entry to the cytoplasm and viral genomic replication[1,2]. Reovirus is dependent on the translational machinery of infected cells for protein synthesis following release of viral RNA into the cytoplasm.

Early studies indicated reovirus tumor selectivity was linked to inactivation of the PKR-mediated anti-viral response driven by oncogenic transformation events [3,4]. However, the role of PKR inactivation is debated within the field with evidence of reovirus sensitivity being PKR-independent [5,6]. PKR forms part of the cellular integrated stress response (ISR). The ISR centres on the phosphorylation of eIF2a on Ser51 by the kinases Protein Kinase-R (PKR), PKR-like endoplasmic reticulum kinase (PERK), general control non-derepressible 2 (GCN2) and Heme-regulated initiation factor 2 alpha kinase (HRI) [7]. Phosphorylation prevents eIF2a forming the active GTP-bound state and ternary complex formation with Met-tRNA and the 40S ribosome. This phosphorylation can be induced by anti-viral recognition of dsRNA by PKR, amino acid deprivation via GCN2, heme-deprivation via HRI or ER stress signaling via PERK,.

PERK is a component of both the integrated stress response and the unfolded protein response (UPR). The UPR is a tripartite cellular response comprised of the ER transmembrane proteins PERK, IRE1a and ATF6 [8,9]. PERK phosphorylation of eIF2a decreases global protein translation while increasing translation of specific mRNA transcripts, such as ATF4, due to regulatory upstream open reading frames [10,11]. IRE1a riboendonuclease activity splices an unconventional 26 nucleotide intron in XBP1 mRNA leading to translation of active spliced-XBP1 [12]. ATF6 activation is driven by trafficking to the Golgi where cleavage releases the soluble cytoplasmic transcription factor ATF6(N) [13]. Through these three cytoplasmic transcription factors, UPR induction acts to resolve stress and restore normal protein homeostasis in the ER.

While PKR has been shown to play a role in some but not all reovirus-permissive cells [5,14], modulation of global protein synthesis may still occur due to other kinases of the ISR, such as GCN2 and PERK. Studies have shown that reovirus induces ER stress and that this could be targeted as a strategy to increase reovirus efficacy. Early publications in this area

showed reovirus efficacy increased in combination with the proteasomal inhibitor bortezomib [15,16]. More recently, BRAF-MEK inhibition sensitized melanoma to reovirus via increased ER stress [17]. Basic research into reovirus biology indicates that despite a cytoplasmic lifecycle, reovirus exerts profound effects on the ER. Reovirus produces viral factories through reorganisation of cell membranes [18]. Neo-organelle formation is driven by the non-structural proteins σNS and μNS [19] that act to remodel the ER forming viral inclusion structures.

Given the ability of reovirus to induce ER stress, we hypothesised that compounds targeting the UPR may sensitize cancer to reovirus. We identified that the PERK inhibitor, GSK2606414, can sensitize head and neck cancer cells to reovirus. GSK2606414 enhanced both reovirus protein production and reovirus-positive areas modelled in 3D spheroids. Profiling of UPR pathways revealed this increase correlated with elevated signaling through eIF2a and ATF4. This eIF2a-ATF4 signal was context dependent, only occurring due to the combination of reovirus and GSK2606414, not the canonical ER stress agent thapsigargin and GSK2606414. Use of shRNA against eIF2a kinases revealed PERK or GCN2 as the kinases responsible for increased eIF2a-ATF4 pathway activity. Knockdown by shRNA confirmed ATF4 was necessary for the GSK2606414 induced increase in reovirus protein levels.

Results

Inhibition of PERK sensitizes HNSCC to reovirus

The HPV-negative head and neck squamous cell carcinoma (HNSCC) cell lines HN5 (tongue) and FaDu (hypopharynx) were used, both are characterised by TP53 mutations and high EGFR and HER2 levels [20]. Survival experiments in 2D identified the PERK inhibitor GSK260414 sensitized FaDu and HN5 cells to reovirus across a range of viral MOIs (Fig. 1A). Values shown are corrected for drug only toxicity. To assess drug-reovirus combination effects, Bliss independence analysis was carried out (Fig. 1B). Greater than expected cell kill was observed when single agent activity was compared to cell kill in combination. Reovirus MOIs of 20 and 75 were selected for FaDu and HN5 cells, respectively, due to these doses falling at the mid-point where combination efficacy was observed. These were used for all subsequent 2D and 3D assays.

The ability of GSK2606414 to increase the efficacy of reovirus was assessed in 3D tumor spheroids. 3D models were used to augment 2D assays as 3D models are both a more clinically relevant method to model stress and were viewed as an approach to modelling the area of viral infection. Fluorescent ubiquitination cell cycle indicator-expressing [21] FaDu and HN5 cells were used to allow a more accurate assessment of spheroid area than brightfield images alone. Representative images after 7 days of GSK2606414 and reovirus infection are shown (Fig. 1C). Spheroids were imaged over 11 days after the addition of GSK2606414 and reovirus. Automated image quantification of spheroid area based on fluorescence from multiple experiments is shown (Fig. 1D). GSK2606414 enhanced the efficacy of reovirus as measured by a reduction in spheroid area. Bliss independence analysis showed greater than expected reduction in volume due to combination treatment compared to single agents alone (Fig 1E). Efficacy *in vivo* was confirmed using both Tet-inducible PERK shRNA (shPERK) knockdown (Fig. 1F) and GSK2606414 in combination with reovirus (Fig 1G). Tumour volume reduction by reovirus was significantly higher in the shPERK group compared to scrambled knockdown (shSCR) control, and in combination with GSK2606414. Validation of PERK knockdown *in vivo,* efficacy of PERK knockdown in combination with reovirus *in vitro,* and *in vivo* curves in mm^3 are shown in supplementary figure S1.

GSK2606414 but not PERK knockdown increases reovirus protein levels *in vitro* and *in vivo*

After confirming increased reovirus efficacy in combination with GSK2606414, we investigated the impact of GSK2606414 on reovirus replication. Reovirus capsid protein

levels were assessed in 2D culture by western blot (Fig. 2A), and reovirus particle production by TCID50 (Fig. 2B). GSK2606414 increased the levels of capsid proteins σ3 and μ1C (Fig. 2A). GSK2606414 also increased viable reovirus particle production by TCID50, although this result was not statistically significant. It can be stated that viable reovirus particle production remains, at a minimum, undiminished despite decreasing cell viability in combination with GSK2606414.

To probe the effects of GSK2606414 in comparison to PERK knockdown, we used 3D tumour spheroids to model the area of reovirus infection. Tumors at the end of *in vivo* experiments in figure 1F and 1G were also assessed for reovirus by IHF. Spheroids were treated with GSK2606414 and reovirus concurrently. After 96 h spheroids were formalin-fixed, paraffin embedded and sectioned. Sections were stained for σ3 and μ1C by fluorescence-based immunohistochemistry (IHF) and confocal images quantified by automated image analysis. An overview of the image analysis pipeline is shown (Fig. 2C). Image segmentation was restricted to the peripheral edge of spheroid corresponding to a depth of 25 μm. This approach was taken due to localisation of the majority of reovirus infection to the spheroid periphery. 3D spheroid sections indicated GSK2606414 enhanced the area that stained positive for reovirus infection as measured by μ1C (Fig. 2D) and σ3 (Fig. 2E). This could be attributed to an increase in the total number of infected cells due to GSK2606414, or an increase in reovirus capsid levels in cells at an early stage in infection compared to reovirus only conditions. Tet inducible knockdown was used as described for figure 1. PERK knockdown by 96 h pre-treatment with doxycycline to induce scrambled or PERK shRNA did not alter the percentage area positive for reovirus in 3D spheroids (Fig 2E). Quantification of reovirus-positive areas at day 18 and day 20, respectively, from GSK2606414 or PERK knockdown *in vivo* experiments showed an increase due to GSK2606414 but not PERK knockdown, similar to observations *in vitro* (Fig 2F). These analyses indicated that while both PERK knockdown and GSK2606414 enhance tumor control by reovirus, only GSK2606414 quantifiably increased reovirus protein levels.

GSK2606414 alters ER chaperone composition in response to reovirus

Reovirus has previously been shown to increase levels of ER-resident chaperones, such as GRP78 and PDI [16]. We sought to assess how GSK2606414 may modulate alterations in ER chaperone levels due to reovirus infection using the same 3D tumor spheroid approach used to model reovirus infection *in vitro* (Figure 3). As in figure 2, spheroids were treated with reovirus and GSK2606414 for 96 h before FFPE processing, sectioning and IHF imaging by

confocal microscopy. Automated image quantification was used to quantify areas of high chaperone expression as outlined for Figure 2C-E. This was isolated to the spheroid periphery as described previously for reovirus infection. In addition, the core of HN5 spheroids displayed high levels of ER chaperones, peripheral quantification excluded changes in this core region not directly linked to reovirus infection (shown in image inset in Fig. 3A).

Representative images are shown for the chaperone GRP78 (Fig. 3A), the ER retention motif KDEL (Fig. 3B) and the chaperone protein disulphide isomerase (PDI) (Fig 3C). GRP78 levels significantly increased following reovirus infection in both cell lines (Fig. 3D). GSK2606414 inhibited GRP78 induction at the edge of spheroids in both cell lines across all doses tested. The ER retention motif, KDEL, was stained to quantify global ER-resident protein levels (Fig. 3E). Reovirus induced an increase in global ER-resident proteins measured by KDEL-high areas that was further increased in combination with GSK2606414. Similar to KDEL, PDI high levels increased due to reovirus infection and were further increased by GSK2606414 addition (Fig. 3F). When comparing reovirus capsid staining patterns in Figure 2 to GRP78, KDEL and PDI staining, a degree of co-localisation was only apparent for PDI and capsid proteins in HN5 cells. Staining of GRP78 and KDEL, particularly in FaDu spheroids, was diffuse relative to highly discrete reovirus capsid positive areas. This indicates that stress induced by reovirus may be due to a combination of a bystander effect or also occurs at early stages of infection where capsid proteins are not yet detectable.

Analyses mirroring spheroid data were performed on *in vivo* samples from end of experiment at day 18 and day 20 (supplementary figure S2). GSK2606414 in combination with reovirus *in vivo* strongly mirrored the increase in PDI observed in spheroids, with decreased GRP78 less clear. PERK knockdown did not alter PDI levels due to reovirus, but increased GRP78 alone at an earlier day 12 timepoint, or at day 20 in reovirus-infected areas. These data indicate both PERK knockdown and GSK2606414 can aggravate/alter the ER stress response to reovirus but the resulting profiles, as measured by the GRP78 and the redox chaperone PDI, are clearly divergent.

GSK2606414 reduces signaling through XBP1 and ATF6 while increasing signaling via eIF2a-ATF4

To understand what may be behind this perturbation of ER chaperones, we generated reporter constructs to investigate the three UPR signaling pathways responsible for regulating chaperone levels. An IRE1a endonuclease reporter contained the 26nt intron from

XBP1 in front of GFP. Splicing and removal of this intron, as is the case with XBP1 to spliced-XBP1, placed GFP in frame (IRE1alpha endonuclease reporter). Downstream of PERK and eIF2a, the 5' upstream regulatory sequence of ATF4 was cloned in front of the start codon of mCherry (ATF4 promoter). Multiple repeats of the previously published ATF6 transcription factor binding site [22] were cloned in front of mCherry (ATF6 reporter). All three are illustrated (Fig. 4A). The canonical ER stress-inducing agent, thapsigargin, was used to validate UPR reporter signaling in combination with GSK2606414 (Fig. 4B). Activation of all UPR reporters by thapsigargin was observed, except for IRE1 reporter activity in FaDu cells. Inhibition of thapsigargin-induced ATF4 reporter levels was clearly observed for GSK2606414, with compensatory increases in other UPR signal pathways (except IRE1 in FaDu cells).

After reporter validation, ATF4, IRE1 and ATF6 reporter levels were imaged after 72h of reovirus infection and GSK2606414 treatment. Representative images are shown (Fig. 4C). Automated image quantification was used to determine reporter intensity across multiple independent experiments (Fig. 4D). No activation of the three arms of the UPR was observed due to reovirus in FaDu spheroids, while ATF6 and ATF4 activity was observed in HN5 spheroids. Though some degree of activation of ATF4 by reovirus was observed in later experiments (see Figure 5B-E). The most pronounced difference was an increase in ATF4 reporter levels due to GSK2606414 alone. This was highly pronounced in FaDu cells. ATF4 reporter levels increased further due to the combination of reovirus and GSK2606414 in HN5 cells alone. To validate signaling upstream from ATF4, levels of pSer51 eIF2a were determined from 2D cell lysates by western blot (Fig. 4E). Densitometry from at least three independent blots is also shown (Fig. 4F). The pattern of pSer51 eIF2a was similar to that observed with the ATF4 reporter. These data indicated that signaling through eIF2a-ATF4 appeared to be the main mechanistic change in UPR signaling during exposure to GSK2606414 and reovirus infection.

Increased reovirus protein levels due to GSK2606414 are ATF4-dependent and due to increased signaling via PERK and GCN2

In the comparison between thapsigargin and reovirus in Figure 4, we noted that the effect of GSK2606414 was context-dependent. Thapsigargin is a much stronger activator of UPR signaling than reovirus, In this context, GSK2606414 strongly inhibits ATF4 protomer activity. However, in the thapsigargin experiment (Fig. 4B), as well as with reovirus (Fig. 4C) we noted GSK2606414 alone caused an increase in ATF4 reporter signaling. Western blot

data (Fig. 4F) indicated that upstream pSer51 eIF2a levels correlated to ATF4 reporter levels. Based on previous data relating to reovirus and the integrated stress response [23], we believed that this may be responsible for the increase in reovirus protein production and infection. To help elucidate the mechanism behind this, doxycycline-inducible shRNA against the integrated stress response eIF2a kinases, PERK, GCN2 and PKR were used (shRNA validation Fig. 5A).

The ATF4 reporter was combined with scrambled, PERK, GCN2 or PKR shRNA and the experiments of figure 4 were repeated. Knockdown of each eIF2a kinase was used to determine the source of ATF4 reporter activity (Fig. 5B,C). All 4 shRNA variants were tested in the absence of doxycycline (black circles) and shown to have similar results to earlier non-shRNA cell lines in figure 4. Induction of scrambled shRNA with doxycycline (blue squares) was shown to have no effect on ATF4 reporter activity due to GSK2606414 and/or reovirus compared to no doxycycline control conditions. Doxycycline-induced knockdown of PERK reduced ATF4 reporter activity in all conditions in FaDu cells. This was most pronounced in GSK2606414 treatment conditions. No reduction was observed in HN5 cells. Doxycycline-induced knockdown of GCN2 was seen to reduce ATF4 reporter activity in all conditions in HN5 cells. While a small decrease was seen in FaDu cells, this was not statistically significant. Doxycycline-induced knockdown of PKR significantly reduced the ATF4 reporter signal in HN5 cells treated with the combination of GSK2606414 and reovirus.

In the context of previous comparative data between PERK knockdown and GSK2606414 (Fig. 2, Supplementary Fig. S2), it is clear that PERK knockdown alone does not increase ATF4 reporter activity in either FaDu or HN5 cells (Fig. 5B,C). This was a mechanistically distinct difference between PERK knockdown and GSK26006414 and potentially the reason behind the disparate effects observed when assessing reovirus levels in figure 2.

To test if increasing pSer51 eIF2a levels (Fig. 4E,F) and ATF4 reporter levels (Fig. 4D; Fig. 5B-E) due to GSK2606414 was the key driver behind increased reovirus protein levels, doxycycline-induced knockdown of ATF4 was used (ATF4sh). Knockdown was validated at the mRNA level by PCR (Fig. 5D). Transcript variant 2 was detectable in both cells, with mRNA levels significantly reduced with doxycycline treatment. ATF4sh blocked increased reovirus μ1C levels due to GSK2606414 (Fig. 5E). Unlike in combination with thapsigargin, in the context of reovirus infection, GSK2606414 can increase signaling through eIF2a-ATF4. ATF4sh confirmed this signaling event as the reason behind increased reovirus protein replication due to GSK2606414. As an additional confirmation, we tested if the potent induction of ATF4 reporter activity observed in figure 4B by thapsigargin alone could also

increase reovirus levels. This proved to be the case (Fig. 5F) suggesting conditions which enhance ATF4 activity have positive consequences for reovirus protein production.

GSK2606414 increases GM-CSF secretion in combination with reovirus

To assess the impact of GSK2606414 on reovirus-induced cytokine secretion, an array was used to profile alterations to cytokine secretion *in vitro* in HN5 cells (Fig 6A,B). This indicated changes to a number of cytokines. Most prominent were increased levels of GM-CSF and decreased levels of a number of T-cell chemoattractants such as CXCL9, 10 and 11 as well as decreased CCL5. However

GM-CSF and CXCL10 findings were validated by ELISA in both FaDu and HN5 cells. This confirmed the increase of GM-CSF in combination with reovirus in HN5s (Fig 6C). FaDu cells did not appear to secrete GM-CSF under any conditions, in keeping with other data on radiation which also showed an absence of GM-CSF expression in FaDu cells [24]. A decrease in reovirus induced CXCL10 secretion by GSK2606414 was observed for both FaDu and HN5 cells. It should be noted however that GSK2606414 reduced CXCL10, but the levels in the combination group was still substantially greater than untreated controls. These data indicate that GSK2606414 may aid dendritic cell infiltration and antigen presentation through GM-CSF, but potentially dampen T-cell chemotaxis through reduced levels of the CXCR3 ligands CXCL9-11.

Discussion

Previous publications have shown that inhibition of BRAF or MEK enhanced the efficacy of reovirus via a mechanism involving ER stress [17]. We hypothesised that direct targeting of UPR signaling may present an opportunity to sensitize HNSCC to reovirus. This led us to identify the PERK inhibitor, GSK2606414, as increasing the efficacy of reovirus in HNSCC.

We observed that GSK2606414 increases reovirus protein levels measured by western blot, as well as the area positive for infection in 3D spheroids and *in vivo*. Tripartite UPR signaling reporters were created to allow monitoring of the UPR in 3D. Initial validation with GSK2606414 and thapsigargin was as expected, with ATF4prom activity blocked by GSK2606414. This coincided with a compensatory increase in the IRE1a and ATF6 UPR pathways. Our original expectation was that reovirus would act much the same as thapsigargin. However, this was not the case, with clear differences in UPR signaling due to reovirus compared to thapsigargin. While GSK2606414 blocked canonical thapsigargin-induced eIF2a-ATF4 signaling, single-agent GSK2606414 yielded an increase. This increase was maintained in FaDu cells and further enhanced in HN5 cells following co-treatment with reovirus. The effect of GSK2606414 was, therefore, context-dependent. In a search of the literature, we were able to corroborate these findings. Single-agent GSK2606414 has been shown previously to increase pSer51 eIF2a [25], although this specific observation was not discussed in that study. To our knowledge, this is the first commentary on this observed phenotype in the literature.

In vivo and *in vitro* data indicated PERK knockdown or GSK2606414 increased tumor control by reovirus, yet the profile of ER stress markers differed. PERK knockdown clearly increased GRP78 levels at day 12 *in vivo*, and increased GRP78 levels in reovirus-infected areas, as well as adjacent areas likely to be in the early stages of infection. Upregulation of GRP78 is a marker of UPR induction and elevated stress. This aggravated stress appears mechanistically different to GSK2606414. Yet either aggravation or perturbation of ER stress signaling by PERK knockdown or GSK260414, respectively, appear to share the same therapeutically beneficial outcome. PERK knockdown failed observably to increase reovirus levels as shown for GSK2606414. These data are in keeping with the identified ATF4-dependent mechanism as PERK knockdown does not induce ATF4 reporter signaling. The precise contribution of these quantifiably increased reovirus metrics to efficacy is difficult to determine. It is logical to conclude that conditions whereby anti-tumor efficacy coincides with increased reovirus persistence is anticipated to be a more therapeutically beneficial scenario.

Activation of the integrated stress response has been associated with a cellular environment supportive of reovirus replication [23]. Isogenic pairs of murine embryonic fibroblasts (MEFs) rather than cancer cell lines were studied, but a possible role in therapeutic efficacy was not investigated. In that study, reovirus replication was not altered in PERK knockout MEFs but was reduced by ATF4 knockout. Our data in a therapeutic context agree with these findings. Increased eIF2a-ATF4 signaling activity due to GSK2606414 corresponded to increased reovirus protein levels with ATF4 knockdown abolishing this increase.

To determine the mechanism behind the increase in eIF2a-ATF4 activity due to GSK2606414, shRNAs against the eIF2a kinases PERK, GCN2 and PKR were used in combination with an ATF4 reporter (Fig. 5B,C). In FaDu cells, ATF4 reporter activity triggered by GSK2606414 was PERK-dependent, whereas in HN5 cells enhanced reporter activity was GCN2-dependent across all conditions, with PKR contributing only when reovirus was combined with GSK2606414. PERK, GCN2 and PKR all form dimers upon activation [26-28]. A recent publication has shown that PERK interacts with the actin regulator FLNA, independent of UPR signaling [29]. In that study, PERK-null cells were reconstituted with PERK lacking the luminal domain. This clearly showed the ability of GSK2606414 to induce PERK dimerization independent of the luminal domain and without the need for thapsigargin treatment. The interaction of PERK-FLNA increased on treatment with GSK2606414, indicating that PERK dimerization and not just kinase activity is sufficient to drive this protein-protein interaction. It is plausible that in the context of reovirus infection, a similar mechanism of action may contribute to the phenotype we observe in this study.

The initial discovery that PERK inhibitors stabilised dimerization was made in the context of a structural similarity to RAF inhibitor-driven kinase dimerization [30]. Inhibitors of wild-type BRAF can drive activation of mutant RAS independently of kinase activity [31-33]. RAF can form homodimers or heterodimers with drug binding inhibiting one subunit of the dimer but inducing transactivation of the other [33]. In Lavoie et al, they concluded that PERK inhibition may result in transactivation of structurally similar GCN2, PKR or HRI, although eIF2a kinase heterodimers have not been reported in the literature. The PERK-dependent increase in ATF4 activity due to GSK2606414 observed in FaDu cells would be in keeping with such transactivation [30] and dimerization events [29]. This suggests a mode of action where GSK2606414 in the context of reovirus infection enhances eIF2a-ATF4 signaling supporting enhanced viral protein production.

The lack of PERK dependence in HN5 cells does not fit this model, but, due to the structural similarity of GCN2 to PERK, it is not inconceivable that some degree of off-target transactivation of GCN2 could be induced by GSK2606414 at the concentrations used. That this was not also observed in FaDu cells may be due to sub-optimal knockdown of GCN2 as a non-significant decrease in GSK2606414 conditions was observed. It has been shown that GSK2606414 has off-target inhibitory effects, notably on RIPK1 [34] and cKIT [35]. In experiments comparing RIPK1 inhibitors to GSK2606414 and thapsigargin (supplementary figure S3), increased reovirus protein levels due to GSK206414 did not appear to be linked to off-target RIPK1 inhibitory effects. Knockdown data on PERK, GCN2 and ATF4 suggests that the effects observed in this study are isolated to UPR signaling alone.

In conclusion, our study reveals GSK2606414 modulates UPR signaling in combination with reovirus in a fashion that is mechanistically different to the canonical ER stress-inducing agent thapsigargin. The context-dependent modulation of UPR signaling due to GSK2606414 allows increased translation of reovirus proteins in an ATF4-dependent manner. This can lead to an increase in the area positive for reovirus infection as modelled in 3D spheroids and *in vivo*. This suggests that future clinical translation should investigate the role of ER stress and in particular ATF4 in profiling susceptibility to reovirus. Combinations of reovirus and agents that enhance ER stress signaling through ATF4 should be considered for future clinical studies.

Materials and Methods

Cell culture and compounds. FaDu and 293T cells were purchased from ATCC. LON-LICR-HN5 cell lines from Professor Sue Eccles (ICR, London, UK). Cells were cultured in DMEM, 5% FBS, 1% (v/v) glutamine, and 0.5% (v/v) penicillin/streptomycin. STR profiling was carried out by Bio-Synthesis Inc. Mycoplasma testing used the e-Myco PCR kit (Intron Biotechnology). Experiments were carried out within 3 months of resuscitation. GSK2606414 was obtained from MedKoo Biosciences (NC, USA). Doxycycline hyclate was obtained from Sigma Aldrich (Gillingham, UK). Reovirus type 3 Dearing (Reolysin/pelarorep) was kindly supplied by Oncolytics Biotech (Calgary, Canada).

MTT viability assay. Cells were seeded in 96-well plates. After 24 h GSK2606414 and reovirus was added concurrently. Viability was determined at 72 hours by MTT assay. Absorbance at 550 nm was measured and viability normalized to control DMSO-treated cells.

3D spheroid size imaging. Cells were plated in ultra-low attachment plates (Corning, #7007). Cells contained cell cycle tracker proteins as previously described [21,36] which were used to visualise spheroid area. Medium was refreshed every 48 h. At 96 h post-plating, GSK2606414 and reovirus were added. GSK2606414 was refreshed every 48 h after addition. Spheroids were imaged at a fixed exposure throughout the experiment on an EVOS FL microscope (ThermoFisher, UK). Spheroid area was quantified by automated image quantification of mCherry and AMCyan channels combined using Cell Profiler v3 (Broad Institute, MA, USA).

Immunoblotting. Cells were scraped in RIPA buffer (ThermoFisher) containing 2 mmol/L Na_3VO_4 and protease inhibitors. Supernatants were quantified by BCA assay (Pierce), separated by SDS-PAGE, transferred to PVDF membrane (ThermoFisher) and blocked in TBS with 5% non-fat dry milk and 0.1% Tween-20. Membranes were probed with the antibodies: pSer51 eIF2a #3398, PERK #5683, GCN2 #3202, PKR #12297, GAPDH #2118 from Cell Signaling Technology (MA, USA); reovirus μ1C 10F6 and reovirus σ3 4F2 were from the Developmental Studies Hybridoma Bank (IA, USA); ATF4 ab184909 and Beta Actin ab8226 were from Abcam (Cambridge, UK).

One-step viral growth $TCID_{50}$ assay. Cells were plated in 24-well plates. After 24 h cells were infected with reovirus with or without GSK2606414. After 2 h media was removed and cells were washed once with PBS. Fresh reovirus free media with or without GSK2606414

was added. Cells and supernatant were harvested and freeze-thawed three times. Resulting supernatants were titred by serial dilution on L929 cells as previously described [37].

Immunofluorescence. Spheroids were rinsed in PBS before fixation in 10% neutral buffered formalin (NBF). Spheroids were embedded in histogel before paraffin-embedding and sectioning. *In vivo* tumors were fixed in NBF before paraffin-embedding and sectioning. Heat-induced antigen retrieval was performed using pH6 sodium citrate buffer. Tissue was blocked using 5 % BSA before incubation with the following antibodies: PERK #5683, GRP78 #3177 and PDI #3501 were from Cell Signaling Technologies (MA,USA); KDEL 10C3 was from Enzo (Exeter, UK); reovirus μ1C 10F6 and reovirus σ3 4F2 were from the Developmental Studies Hybridoma Bank (IA, USA). Alexafluor 488, 546 and 647 conjugates of anti-rabbit IgG H+L, anti-mouse IgG H+L, anti-mouse IgG2a and anti-mouse IgG2b were from ThermoFisher (UK). Spheroid sections were imaged on a Zeiss 710 confocal (Jena, Germany) with quantification using Cell Profiler v3. Exposure settings were based on the minimum possible which still allowed robust spheroid identification for segmentation. Controls were compared during exposure setup to ensure similar intensities across experiments. Stained sections from *in vivo* tumor samples were imaged on a Perkin Elmer Vectra 3.0 with spectral unmixing of images performed using Perkin Elmer Inform software. Image quantification performed using Cell Profiler v3 as described in results.

Cytokine Profiling. Media 48 h after treatment with reovirus and GSK2606414 was collected and centrifuged to remove cells or debris. Initial profiling used the proteome profiler human XL cytokine array kit from R&D systems (MN, USA). Array results were quantified by densitometry using ImageJ (FIJI v2). Validation of array findings used the human CXCL10/IP-10 Duoset and human GM-CSF Duoset ELISA kits from R&D systems.

UPR reporter constructs and high-content Imaging. Reporter constructs were cloned into the lentivirus pHRSIN (kindly provided by Professor Greg Towers, UCL, London). Primers are listed in supplementary Table S1. The region encoding the 26nt intron from XBP1 excised by IRE1a riboendonuclease activity was incorporated by PCR in front of eGFPFLAG and inserted between SFFV and WPRE elements (LV-IRE1endo). 1800 bp upstream of the ATF4 start codon was amplified from genomic DNA by PCR, with a second PCR referred to as extended primers adding overlap assembly regions at the 5' end for pHRSIN and the 3' end for mCherry. mCherry was amplified by PCR using an initial PCR including a previously cloned C-terminal MYC tag, followed by a second PCR to add a 3' overlap assembly region with pHRSIN. This was assembled into pHRSIN using NEBuilder (NEB, USA) resulting in mCherry with the 5' 1800bp genomic sequence of ATF4 and a 3' WPRE element from

pHRSIN (LV-ATF4prom). Using the previously published ATF6 binding site [22] 5-repeats of the binding site (addgene ID 11976) were inserted in front of eGFP-WPRE (LV-ATF6bind). Lentiviral reporter constructs were packaged using MD2.G and psPAX2 in 293T cells using lipofectamine 2000. Supernatants containing polybrene were used to infect cell lines with reporter constructs individually and selected using puromycin or blasticidin. Reporter expression was measured using a Celigo S high-content imaging system from Nexcelom Bioscience (MA, USA). Spheroid recognition and average reporter intensity was quantified using Cell Profiler v3.

Tet-pLKO-puro shRNA. Short hairpin RNA sequences for scrambled, PERK, GCN2, PKR and ATF4 were cloned into the Tet-pLKO-puro system [38]. Target sequences: scrambled, GACAAGTTAAGAACCGCGA; PERK, CCGTGAAAGCATGGAAACA; GCN2, TGGCTAAGCAGGAACGTTT; PKR, GGGCTAATTCTTGCTGAAC; ATF4, TGCTTACGTTGCCATGATC. Knockdown was validated after 96 h in 400 μg/mL doxycycline with fresh doxycycline added at 48 h. In all experiments, doxycycline was refreshed every 48 h until the end of the experiment. GSK2606414 and reovirus addition took place after 96 h of pre-treatment with doxycycline. Validation by western blot, except for ATF4 which was by PCR. For PCR validation, RNA was prepped using an RNeasy Plus kit (Qiagen), converted to cDNA using Protoscript II (NEB), with PCR performed using GoTaq DNA polymerase (Promega). ATF4 transcript variant 1 and 2 primers are listed in supplementary table 2. In studies combining Tet-pLKO-puro shRNA with LV-ATF4prom, puromycin and blasticidin were used sequentially for selection of positively infected cells. Imaging and quantitation as outlined previously for UPR reporters.

In vivo. All experiments were approved by the Institutional Ethics Review Board. Female NOD scid gamma (NSG) mice were obtained from Charles River, 2 million HN5 cells were implanted subcutaneously. HN5 cells were parental, or contained Tet-pLKO-puro SCR shRNA or PERK-targeting shRNA. Scrambled shRNA groups contained n=6 mice, PERK shRNA n=5. Doxycycline in 5% dextrose was given once daily by oral gavage for the duration of the experiment to all groups. Reovirus was injected intratumorally as $1x10^5$ plaque forming units in a volume of 30 μL of PBS on day zero. Sham injection consisted of PBS only. GSK2606414 50 mg/kg or vehicle was administered via oral gavage once per day using a 5 days on, 2 days off schedule commencing on day zero. Vehicle was 0.5% hydroxypropyl methylcellulose and 0.1% Tween 80. Reovirus was injected intratumorally as $1x10^5$ plaque forming units in a volume of 30 μL of PBS on day zero, and

$1x10^7$ in 30 μL of PBS on day nine. Sham injection consisted of PBS only. Tumor diameters were measured by vernier calipers and volume calculated as (width x width x length)/2.

Acknowledgements: This study was supported by The Oracle Cancer Trust (MM), The Oracle Cancer Trust Mark Donegan Fellowship (VR, JK), GetAhead (KB), RM/ICR NIHR Biomedical Research Centre, Rosetrees Trust (MTD, KJH, grant numbers M48 and M444), Cancer Research United Kingdom (MP, AM) and Anthony Long Charitable Trust (KJH). The authors declare no potential conflicts of interest.

Author Contributions:

Conceptualization, MM and KJH; Methodology, MM, MP, VR, KB, HGS, JK, MTD; Investigation, MM, MP, KB, HGS, HW; Writing and review, MM, HP, RV, AM, KJH; Supervision, KJH.

1. Forrest, JC, Campbell, JA, Schelling, P, Stehle, T and Dermody, TS (2003). Structure-Function Analysis of Reovirus Binding to Junctional Adhesion Molecule 1. *J. Biol. Chem.* **278**: 48434–48444.
2. Maginnis, MS, Forrest, JC, Kopecky-Bromberg, SA, Dickeson, SK, Santoro, SA, Zutter, MM, *et al.* (2006). Beta1 integrin mediates internalization of mammalian reovirus. *Journal of Virology* **80**: 2760–2770.
3. Strong, JE, Tang, D and Lee, PW (1993). Evidence that the epidermal growth factor receptor on host cells confers reovirus infection efficiency. *Virology* **197**: 405–411.
4. Strong, JE, Coffey, MC, Tang, D, Sabinin, P and Lee, PW (1998). The molecular basis of viral oncolysis: usurpation of the Ras signaling pathway by reovirus. *EMBO J.* **17**: 3351–3362.
5. Twigger, K, Roulstone, V, Kyula, J, Karapanagiotou, EM, Syrigos, KN, Morgan, R, *et al.* (2012). Reovirus exerts potent oncolytic effects in head and neck cancer cell lines that are independent of signalling in the EGFR pathway. *BMC Cancer* **12**: 368.
6. Smakman, N, van den Wollenberg, DJM, Borel Rinkes, IHM, Hoeben, RC and Kranenburg, O (2005). Sensitization to apoptosis underlies KrasD12-dependent oncolysis of murine C26 colorectal carcinoma cells by reovirus T3D. *Journal of Virology* **79**: 14981–14985.
7. Pakos-Zebrucka, K, Koryga, I, Mnich, K, Ljujic, M, Samali, A and Gorman, AM (2016). The integrated stress response. *EMBO Rep.* **17**: 1374–1395.
8. Walter, P and Ron, D (2011). The Unfolded Protein Response: From Stress Pathway to Homeostatic Regulation. *Science* **334**: 1081–1086.
9. Hetz, C and Papa, FR (2018). The Unfolded Protein Response and Cell Fate Control. *Mol. Cell* **69**: 169–181.
10. Vattem, KM and Wek, RC (2004). Reinitiation involving upstream ORFs regulates ATF4 mRNA translation in mammalian cells. *Proc Natl Acad Sci USA* **101**: 11269–11274.
11. Chan, C-P, Kok, K-H, Tang, H-MV, Wong, C-M and Jin, D-Y (2013). Internal ribosome entry site-mediated translational regulation of ATF4 splice variant in mammalian unfolded protein response. *Biochim. Biophys. Acta* **1833**: 2165–2175.
12. Yoshida, H, Matsui, T, Yamamoto, A, Okada, T and Mori, K (2001). XBP1 mRNA Is Induced by ATF6 and Spliced by IRE1 in Response to ER Stress to Produce a Highly Active Transcription Factor. *Cell* **107**: 881–891.
13. Ye, J, Rawson, RB, Komuro, R, Chen, X, Davé, UP, Prywes, R, *et al.* (2000). ER Stress Induces Cleavage of Membrane-Bound ATF6 by the Same Proteases that Process SREBPs. *Mol. Cell* **6**: 1355–1364.
14. Smith, JA, Schmechel, SC, Williams, BRG, Silverman, RH and Schiff, LA (2005). Involvement of the interferon-regulated antiviral proteins PKR and RNase L in reovirus-induced shutoff of cellular translation. *Journal of Virology* **79**: 2240–2250.
15. Kelly, KR, Espitia, CM, Mahalingam, D, Oyajobi, BO, Coffey, M, Giles, FJ, *et al.* (2012). Reovirus therapy stimulates endoplasmic reticular stress, NOXA induction, and augments bortezomib-mediated apoptosis in multiple myeloma. *Oncogene* **31**: 3023–3038.
16. Carew, JS, Espitia, CM, Zhao, W, Kelly, KR, Coffey, M, Freeman, JW, *et al.* (2013). Reolysin is a novel reovirus-based agent that induces endoplasmic reticular stress-mediated apoptosis in pancreatic cancer. *Cell Death Dis.* **4**: e728.
17. Roulstone, V, Pedersen, M, Kyula, J, Mansfield, D, Khan, AA, McEntee, G, *et al.* (2015). BRAF- and MEK-Targeted Small Molecule Inhibitors Exert Enhanced Antimelanoma Effects in Combination With Oncolytic Reovirus Through ER Stress. *Mol. Ther.* **23**: 931–942.
18. Fernandez de Castro, I, Zamora, PF, Ooms, L, Fernandez, JJ, Lai, CMH, Mainou, BA, *et al.* (2013). Reovirus Forms Neo-Organelles for Progeny Particle Assembly within Reorganized Cell Membranes. *mBio* **5**: e00931–13.

19. Tenorio, R, Fernández de Castro, I, Knowlton, JJ, Zamora, PF, Lee, CH, Mainou, BA, *et al.* (2018). Reovirus σNS and μNS Proteins Remodel the Endoplasmic Reticulum to Build Replication Neo-Organelles. In: Griffin, DE (ed.). *mBio* **9**: e01253–18.
20. Rogers, SJ, Box, C, Chambers, P, Barbachano, Y, Nutting, CM, Rhŷs-Evans, P, *et al.* (2009). Determinants of response to epidermal growth factor receptor tyrosine kinase inhibition in squamous cell carcinoma of the head and neck. *J. Pathol.* **218**: 122–130.
21. Sakaue-Sawano, A, Kurokawa, H, Morimura, T, Hanyu, A, Hama, H, Osawa, H, *et al.* (2008). Visualizing spatiotemporal dynamics of multicellular cell-cycle progression. *Cell* **132**: 487–498.
22. Wang, Y, Shen, J, Arenzana, N, Tirasophon, W, Kaufman, RJ and Prywes, R (2000). Activation of ATF6 and an ATF6 DNA binding site by the endoplasmic reticulum stress response. *J. Biol. Chem.* **275**: 27013–27020.
23. Smith, JA, Schmechel, SC, Raghavan, A, Abelson, M, Reilly, C, Katze, MG, *et al.* (2006). Reovirus induces and benefits from an integrated cellular stress response. *Journal of Virology* **80**: 2019–2033.
24. Dillon, MT, Bergerhoff, KF, Pedersen, M, Whittock, H, Crespo-Rodriguez, E, Patin, EC, *et al.* (2019). ATR Inhibition Potentiates the Radiation-induced Inflammatory Tumor Microenvironment. *Clinical Cancer Research* **25**: 3392–3403.
25. Guthrie, LN, Abiraman, K, Plyler, ES, Sprenkle, NT, Gibson, SA, McFarland, BC, *et al.* (2016). Attenuation of PKR-like ER Kinase (PERK) Signaling Selectively Controls Endoplasmic Reticulum Stress-induced Inflammation Without Compromising Immunological Responses. *J. Biol. Chem.* **291**: 15830–15840.
26. He, H, Singh, I, Wek, SA, Dey, S, Baird, TD, Wek, RC, *et al.* (2014). Crystal structures of GCN2 protein kinase C-terminal domains suggest regulatory differences in yeast and mammals. *J. Biol. Chem.* **289**: 15023–15034.
27. Dey, M, Cao, C, Dar, AC, Tamura, T, Ozato, K, Sicheri, F, *et al.* (2005). Mechanistic link between PKR dimerization, autophosphorylation, and eIF2alpha substrate recognition. *Cell* **122**: 901–913.
28. Cui, W, Li, J, Ron, D and Sha, B (2011). The structure of the PERK kinase domain suggests the mechanism for its activation. *Acta Crystallogr. D Biol. Crystallogr.* **67**: 423–428.
29. van Vliet, AR, Giordano, F, Gerlo, S, Segura, I, Van Eygen, S, Molenberghs, G, *et al.* (2017). The ER Stress Sensor PERK Coordinates ER-Plasma Membrane Contact Site Formation through Interaction with Filamin-A and F-Actin Remodeling. *Mol. Cell* **65**: 885–899.e6.
30. Lavoie, H, Thevakumaran, N, Gavory, G, Li, JJ, Padeganeh, A, Guiral, S, *et al.* (2013). Inhibitors that stabilize a closed RAF kinase domain conformation induce dimerization. *Nat. Chem. Biol.* **9**: 428–436.
31. Heidorn, SJ, Milagre, C, Whittaker, S, Nourry, A, Niculescu-Duvas, I, Dhomen, N, *et al.* (2010). Kinase-dead BRAF and oncogenic RAS cooperate to drive tumor progression through CRAF. *Cell* **140**: 209–221.
32. Hatzivassiliou, G, Song, K, Yen, I, Brandhuber, BJ, Anderson, DJ, Alvarado, R, *et al.* (2010). RAF inhibitors prime wild-type RAF to activate the MAPK pathway and enhance growth. *Nature* **464**: 431–435.
33. Poulikakos, PI, Zhang, C, Bollag, G, Shokat, KM and Rosen, N (2010). RAF inhibitors transactivate RAF dimers and ERK signalling in cells with wild-type BRAF. *Nature* **464**: 427–430.
34. Rojas-Rivera, D, Delvaeye, T, Roelandt, R, Nerinckx, W, Augustyns, K, Vandenabeele, P, *et al.* (2017). When PERK inhibitors turn out to be new potent RIPK1 inhibitors: critical issues on the specificity and use of GSK2606414 and GSK2656157. *Cell Death Differ.* **24**: 1100–1110.
35. Mahameed, M, Wilhelm, T, Darawshi, O, Obiedat, A, Tommy, W-S, Chintha, C, *et al.* (2019). The unfolded protein response modulators GSK2606414 and KIRA6 are potent KIT inhibitors. *Cell Death Dis.* **10**: 300.

36. Dillon, MT, Barker, HE, Pedersen, M, Hafsi, H, Bhide, SA, Newbold, KL, *et al.* (2017). Radiosensitization by the ATR Inhibitor AZD6738 through Generation of Acentric Micronuclei. *Molecular Cancer Therapeutics* **16**: 25–34.
37. Twigger, K, Vidal, L, White, CL, De Bono, JS, Bhide, S, Coffey, M, *et al.* (2008). Enhanced in vitro and in vivo cytotoxicity of combined reovirus and radiotherapy. *Clinical Cancer Research* **14**: 912–923.
38. Wiederschain, D, Wee, S, Chen, L, Loo, A, Yang, G, Huang, A, *et al.* (2009). Single-vector inducible lentiviral RNAi system for oncology target validation. *Cell Cycle* **8**: 498–504.

Figure 1. GSK2606414 sensitizes HNSCC to reovirus. (A) Cell viability of FaDu and HN5 HNSCC cell lines was determined at 72h by MTT assay. GSK2606414 and reovirus were added concurrently. (B) Observed cell kill vs expected cell kill for MTT assays was determined by Bliss independence analysis. Expected cell kill is calculated on the assumption single agents are non-interacting. Positive ΔE corresponds to greater observed kill than expected, negative ΔE less than expected. Full details outlined in methods. (C, D) FaDu and HN5 HNSCC cell lines were plated in low attachment U-bottom plates to form 3D tumour spheroids expressing G1-mCherry and G2-AMCyan cell cycle trackers. Spheroids were treated with GSK2606414 and reovirus concurrently. Spheroids were imaged using cell cycle tracker fluorescence at the indicated time points. Area relative to control was calculated by automated image quantification. (E) Observed reduction vs expected reduction for 3D spheroid areas was determined by Bliss independence analysis as in panel B. (F) Increased efficacy of reovirus in combination with loss of PERK was determined *in vivo* by Tet-inducible shRNA. HN5 cells stably expressing lentiviral Tet-pLKO-puro were injected subcutaneously into NSG mice. HN5 cells contained either scrambled shRNA (SCRsh) or PERK targeting shRNA (PERKsh). All mice received 50 mg/Kg doxycycline daily by gavage with reovirus delivered by intra-tumoral injection at day zero. Tumor volumes expressed relative to start volume. For validation of knockdown see supplementary figure S1. (G) Increased efficacy of reovirus in combination with GSK2606414 was determined *in vivo* in HN5 cells injected subcutaneously into NSG mice. Mice received 50 mg/kg GSK2606414 on days 0-4, 7-11,14-18 with two injections of reovirus on day zero and day 9. A and D, data ±SEM of at least three independent experiments. Bliss independence analysis in B and E shown with 95% confidence intervals. *In vivo* statistical analysis shown between groups in F and G by unpaired t-test *P < 0.05 of area under curve comparison for individual tumors.

Figure 2. GSK2606414 increases reovirus infection in 2D and modelled in 3D tumor spheroids. (A) Lysates from 2D cell culture at the time points indicated after treatment were probed by western blot for the reovirus capsid proteins μ1C and σ3. (B) Viable replicating reovirus particle production from media and cells combined from 2D culture was quantified by TCID50 assay. (C, D, E) HNSCC cell lines were plated in low attachment U-bottom plates to form spheroids and treated as in Figure 1. 96 h after treatment spheroids were collected, formalin-fixed, paraffin embedded and sectioned. Sections were stained for reovirus μ1C and σ3 by IHF to quantify the area positive for reovirus infection. Confocal images were quantified by automated image quantification of infected areas as illustrated. 20x field of view shown corresponds to 415 x 415 μm. Due to reovirus only accessing and infecting the peripheral edge of the spheroid, quantification was restricted to a depth of 25 μM. Further details on this rationale are outlined in the results section. (E) 3D spheroids containing SCR or PERK shRNA were treated with doxycycline for 96h before infection with reovirus. After a further 96 h in doxycycline, spheroids were collected and stained for reovirus μ1C as described for C-D. (F) FFPE tumors from end of experiment from figure 1F and 1G were sectioned and stained for reovirus μ1C by IHF. Slides were imaged on a Perkin Elmer Vectra 3 and the percentage area positive for reovirus quantified using cell profiler software averaged from two sections. Reovirus-positive areas are expressed as fold change relative to reovirus alone for GSK2606414, or scrambled shRNA for PERK

shRNA knockdown. Spheroid datapoints represent the average of 4-8 spheroids within a single independent experiment. All figure data ±SEM, statistical analysis by unpaired t-test *P < 0.05.

Figure 3. GSK2606414 inhibits reovirus induced GRP78 while increasing PDI and overall ER resident KDEL levels. FaDu and HN5 HNSCC 3D tumor spheroids were treated with GSK2606414 and reovirus for 96h before spheroids were formalin-fixed, paraffin embedded and sectioned. Sections were stained by IHF for (A) GRP78, (B) KDEL and (C) PDI. 20x field of view shown corresponds to 415 x 415 μm. Confocal images were quantified for areas of high expression, restricted to the peripheral 25 μM as previously outlined in figure 2. Quantification for both FaDu and HN5 cells shown for (D) GRP78, (E) KDEL and (F) PDI. Each point represents an independent experiment where each experiment is an average of 4-8 spheroids. Data ±SEM with statistical analysis by unpaired t-test *P < 0.05.

Figure 4. GSK2606414 increases UPR signalling through eIF2a-ATF4 while decreasing signalling through IRE1alpha and ATF6. (A) Illustration of tripartite UPR reporter design for live cell imaging of: IRE1a splicing of XBP1 intron sequence; ATF4 translation downstream of eIF2a; and activity of the ATF6 consensus DNA binding sequence. (B) 3D tumor spheroids containing reporter constructs were treated with 100 nM thapsigargin, 5 μM GSK2606414 and imaged at 72 h to profile lentiviral UPR reporter constructs. To aid clarity, greyscale images are presented using the pseudo-colour scale shown. (C) 3D tumor spheroids containing reporter constructs were treated with reovirus and GSK2606414 and imaged at 72h. (D) Automated image analysis was used to identify spheroids and calculate average reporter intensity. Each data point represents an independent experiment, each containing the average of at least 4 spheroids. (E) 2D cell lysates were collected after 48 h treatment of cells with reovirus and GSK2606414. Lysates were probed for pSer51 EIF2a. (F) Densitometry quantification of pSer51 eIF2a from western blots of three independent experiments. Data is corrected for loading and normalised to control. Data ±SEM of a minimum of three independent experiments with statistical analysis by unpaired t-test *P < 0.05.

Figure 5. In the context of Reovirus infection, GSK2606414 promotes eIF2a-ATF4 signalling via PERK or GCN2 with increased viral protein levels ATF4-dependent. (A) Western blot of cell lysates from 2D culture validating Tet-pLKO shRNA knockdown of PERK, GCN2 and PKR after 96 h of doxycycline treatment. (B-C) FaDu and HN5 cells were co-infected with ATF4-mCherry reporter in combination with Tet-pLKO SCR, PERK, GCN2 or PKR targeting shRNA. Spheroids were treated for 96h with doxycycline before treatment with GSK2606414 and reovirus. Reporter expression was imaged at 72h matching the timepoint used in figure 4. Control values (black circles) are for parental Tet-pLKO cell lines in the absence of doxycycline knockdown, shRNA values (blue squares) correspond to doxycycline induced shRNA expression and knockdown. (D) FaDu and HN5 cells were infected with Tet-pLKO inducible shRNA targeting ATF4 or scrambled control. ATF4 transcript variant 2 but not variant 1 was present in both cell lines. Knockdown after 96 h of doxycycline treatment was confirmed by PCR. Quantitation of PCR band intensity from three independent experiments

expressed relative to SCR control for each cell line. (E) After 96 h of pre-treatment with doxycycline to establish ATF4 knockdown, cells were exposed to reovirus and GSK2606414 for 48 h before analysis of reovirus μ1C protein levels by western blot. (F) Cell were treated with DMSO control, GSK2606414 or thapsigargin in combination with reovirus and analyzed at 48 h for μ1C protein levels by western blot. Data ±SEM of a minimum of three independent experiments with statistical analysis by unpaired t-test *P < 0.05.

Figure 6. GSK2606414 modulates cytokine production in response to reovirus, increasing GM-CSF levels. (A, B) A human cytokine array was used to assess cytokine secretion *in vitro* in response to reovirus in combination with GSK2606414 after 48 h. Only cytokines where changes were observed are shown, with levels quantified and displayed also by heatmap. (C, D) Findings for GM-CSF and CXCL10 were validated by ELISA using media at 48 h. Data ±SEM of a minimum of three independent experiments with statistical analysis by unpaired t-test *P < 0.05.

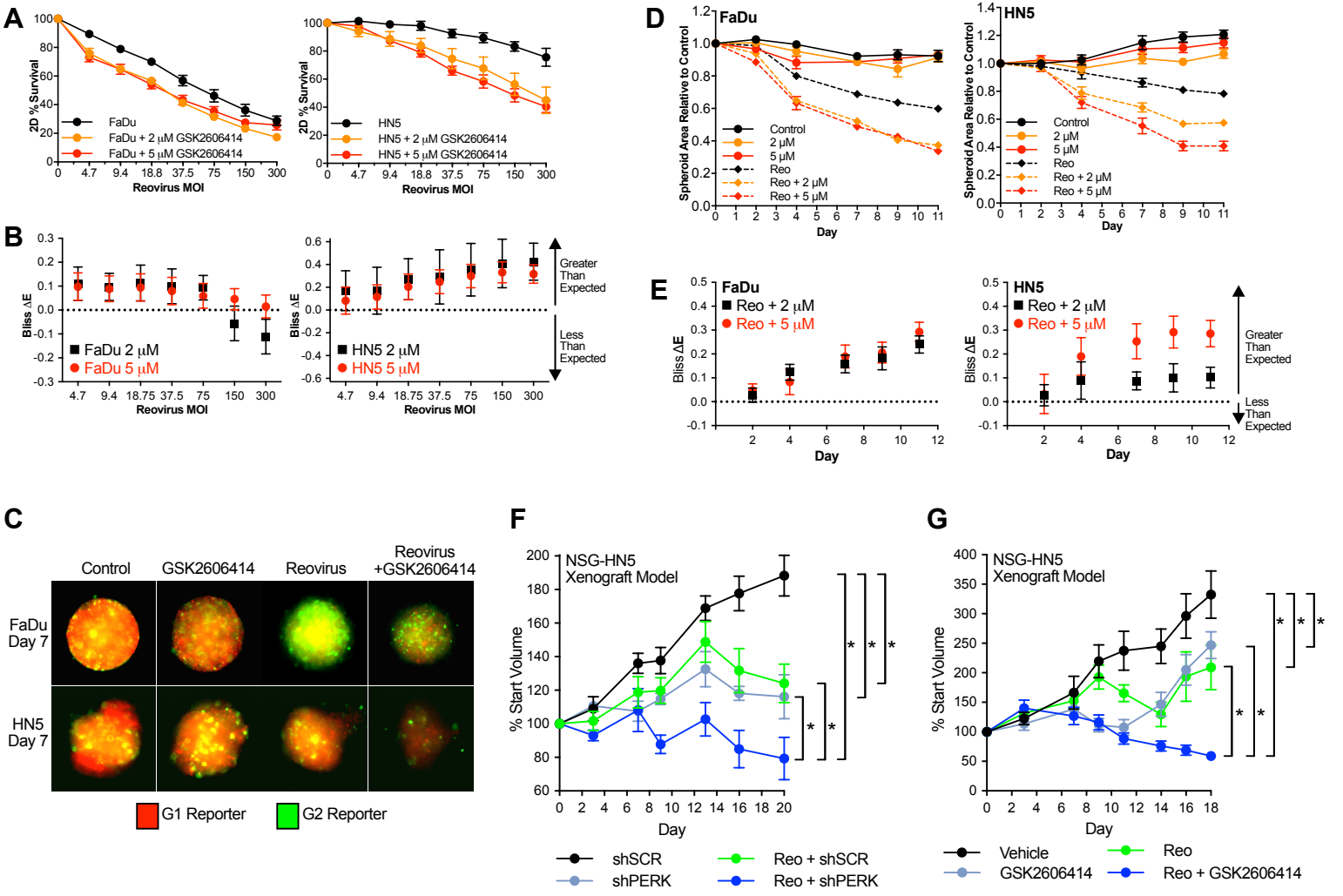
A
2D % Survival
Reovirus MOI
FaDu
FaDu + 2 μM GSK2606414
FaDu + 5 μM GSK2606414
HN5
HN5 + 2 μM GSK2606414
HN5 + 5 μM GSK2606414
B
Bliss ΔE
FaDu 2 μM
FaDu 5 μM
HN5 2 μM
HN5 5 μM
Greater Than Expected
Less Than Expected
C
Control
GSK2606414
Reovirus
Reovirus +GSK2606414
FaDu Day 7
HN5 Day 7
G1 Reporter
G2 Reporter
D
FaDu
HN5
Spheroid Area Relative to Control
Day
Control
2 μM
5 μM
Reo
Reo + 2 μM
Reo + 5 μM
E
FaDu
HN5
Reo + 2 μM
Reo + 5 μM
Bliss ΔE
Day
Greater Than Expected
Less Than Expected
F
NSG-HN5 Xenograft Model
% Start Volume
Day
shSCR
shPERK
Reo + shSCR
Reo + shPERK
G
NSG-HN5 Xenograft Model
% Start Volume
Day
Vehicle
GSK2606414
Reo
Reo + GSK2606414

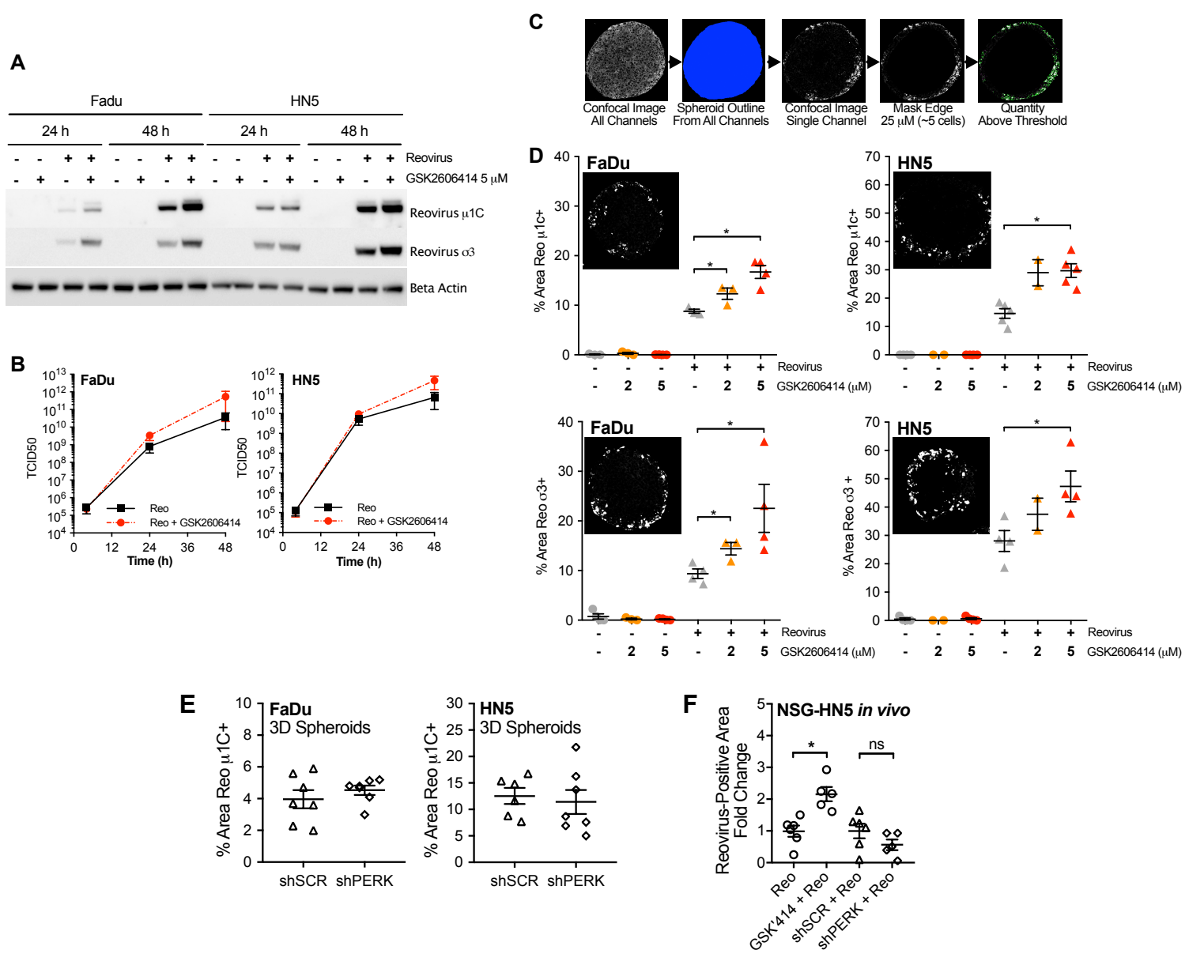
A
Fadu
HN5
24 h
48 h
24 h
48 h
Reovirus
GSK2606414 5 μM
Reovirus μ1C
Reovirus σ3
Beta Actin
B
FaDu
HN5
TCID50
Reo
Reo + GSK2606414
Time (h)
C
Confocal Image All Channels
Spheroid Outline From All Channels
Confocal Image Single Channel
Mask Edge 25 μM (~5 cells)
Quantity Above Threshold
D
FaDu
HN5
% Area Reo μ1c+
% Area Reo σ3+
% Area Reo σ3 +
Reovirus
GSK2606414 (μM)
E
FaDu
3D Spheroids
HN5
3D Spheroids
% Area Reo μ1C+
shSCR
shPERK
F
NSG-HN5 in vivo
Reovirus-Positive Area Fold Change
ns
Reo
GSK'414 + Reo
shSCR + Reo
shPERK + Reo

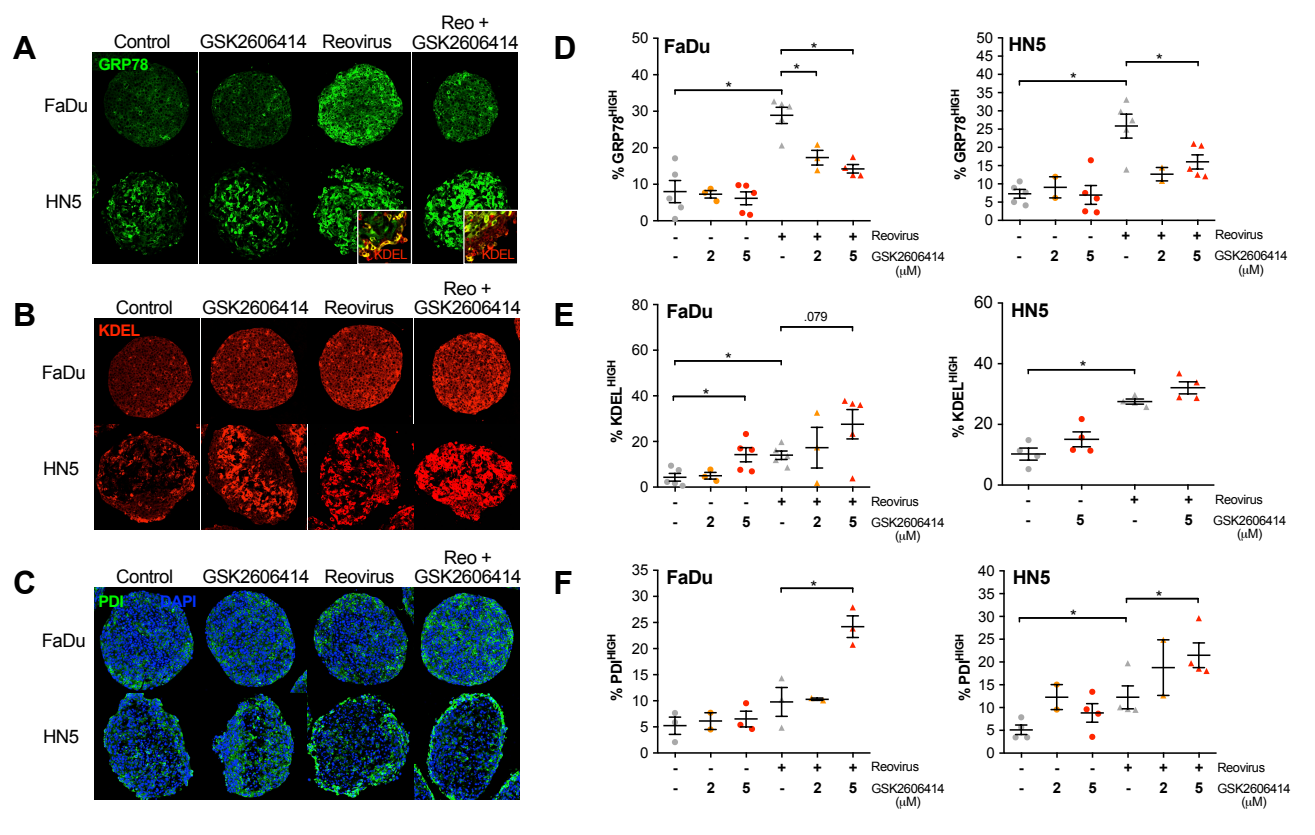
A
Control
GSK2606414
Reovirus
Reo + GSK2606414
GRP78
FaDu
HN5
KDEL
KDEL
B
Control
GSK2606414
Reovirus
Reo + GSK2606414
KDEL
FaDu
HN5
C
Control
GSK2606414
Reovirus
Reo + GSK2606414
PDI
DAPI
FaDu
HN5
D
FaDu
% GRP78HIGH
HN5
% GRP78HIGH
Reovirus
GSK2606414 (μM)
E
FaDu
% KDELHIGH
.079
HN5
% KDELHIGH
Reovirus
GSK2606414 (μM)
F
FaDu
% PDIHIGH
HN5
% PDIHIGH
Reovirus
GSK2606414 (μM)

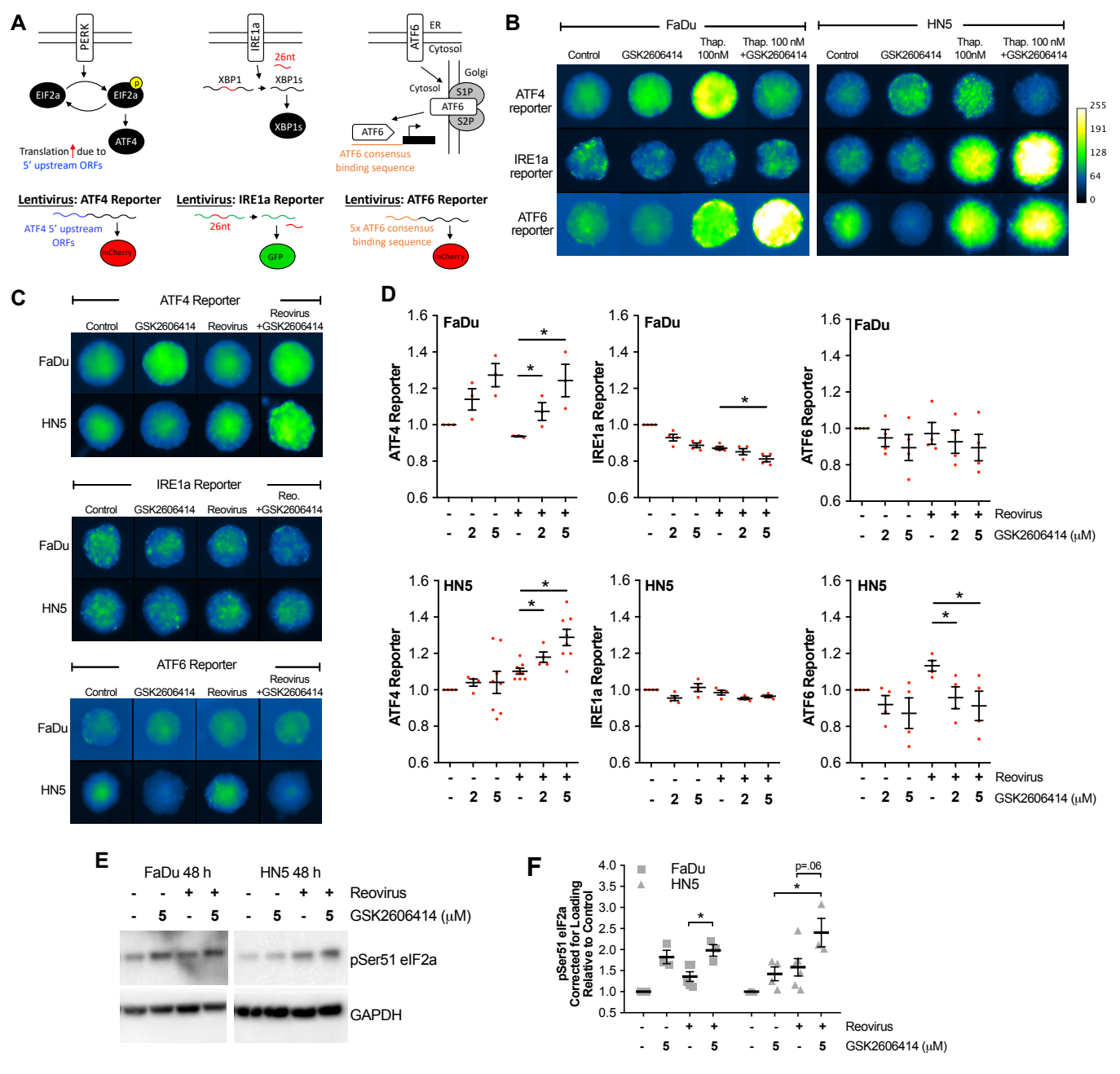
A
PERK
EIF2a
P
EIF2a
ATF4
Translation ↑ due to
5' upstream ORFs
IRE1a
26nt
XBP1
XBP1s
XBP1s
ATF6
ER
Cytosol
Golgi
Cytosol
S1P
ATF6
S2P
ATF6
ATF6 consensus
binding sequence
Lentivirus: ATF4 Reporter
ATF4 5' upstream
ORFs
mCherry
Lentivirus: IRE1a Reporter
26nt
GFP
Lentivirus: ATF6 Reporter
5x ATF6 consensus
binding sequence
mCherry
B
FaDu
HN5
Control
GSK2606414
Thap. 100nM
Thap. 100 nM +GSK2606414
ATF4 reporter
IRE1a reporter
ATF6 reporter
255
191
128
64
0
C
ATF4 Reporter
Control
GSK2606414
Reovirus
Reovirus +GSK2606414
FaDu
HN5
IRE1a Reporter
Reo. +GSK2606414
ATF6 Reporter
D
FaDu
HN5
ATF4 Reporter
IRE1a Reporter
ATF6 Reporter
Reovirus
GSK2606414 (μM)
E
FaDu 48 h
HN5 48 h
Reovirus
GSK2606414 (μM)
pSer51 eIF2a
GAPDH
F
FaDu
HN5
pSer51 eIF2a Corrected for Loading Relative to Control
p=.06
Reovirus
GSK2606414 (μM)

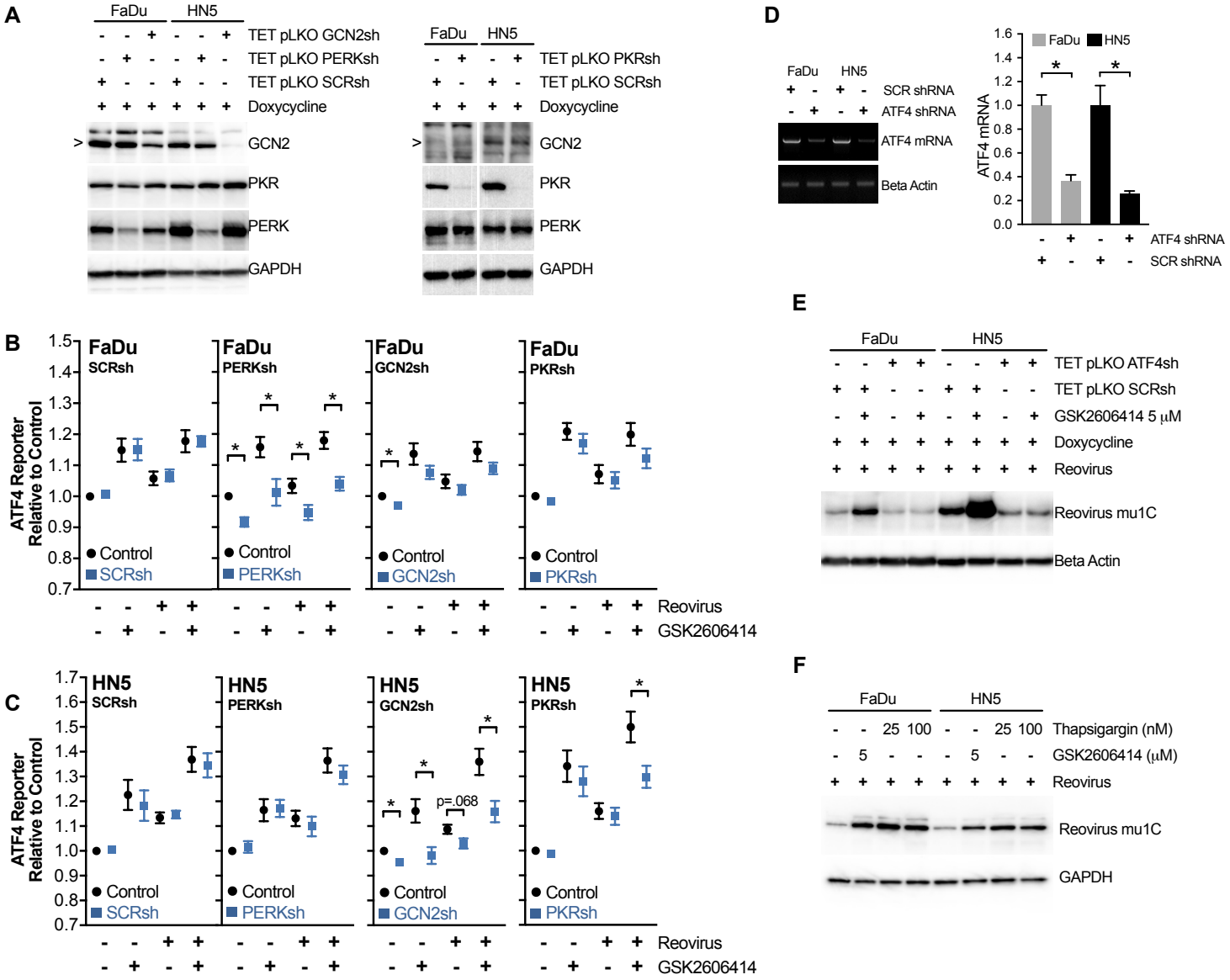
A
FaDu
HN5
TET pLKO GCN2sh
TET pLKO PERKsh
TET pLKO SCRsh
Doxycycline
GCN2
PKR
PERK
GAPDH
TET pLKO PKRsh
B
FaDu
SCRsh
PERKsh
GCN2sh
PKRsh
ATF4 Reporter Relative to Control
Control
SCRsh
PERKsh
GCN2sh
PKRsh
Reovirus
GSK2606414
C
HN5
p=.068
D
SCR shRNA
ATF4 shRNA
ATF4 mRNA
Beta Actin
ATF4 mRNA
E
TET pLKO ATF4sh
TET pLKO SCRsh
GSK2606414 5 μM
Reovirus mu1C
Beta Actin
F
Thapsigargin (nM)
GSK2606414 (μM)
Reovirus mu1C
GAPDH

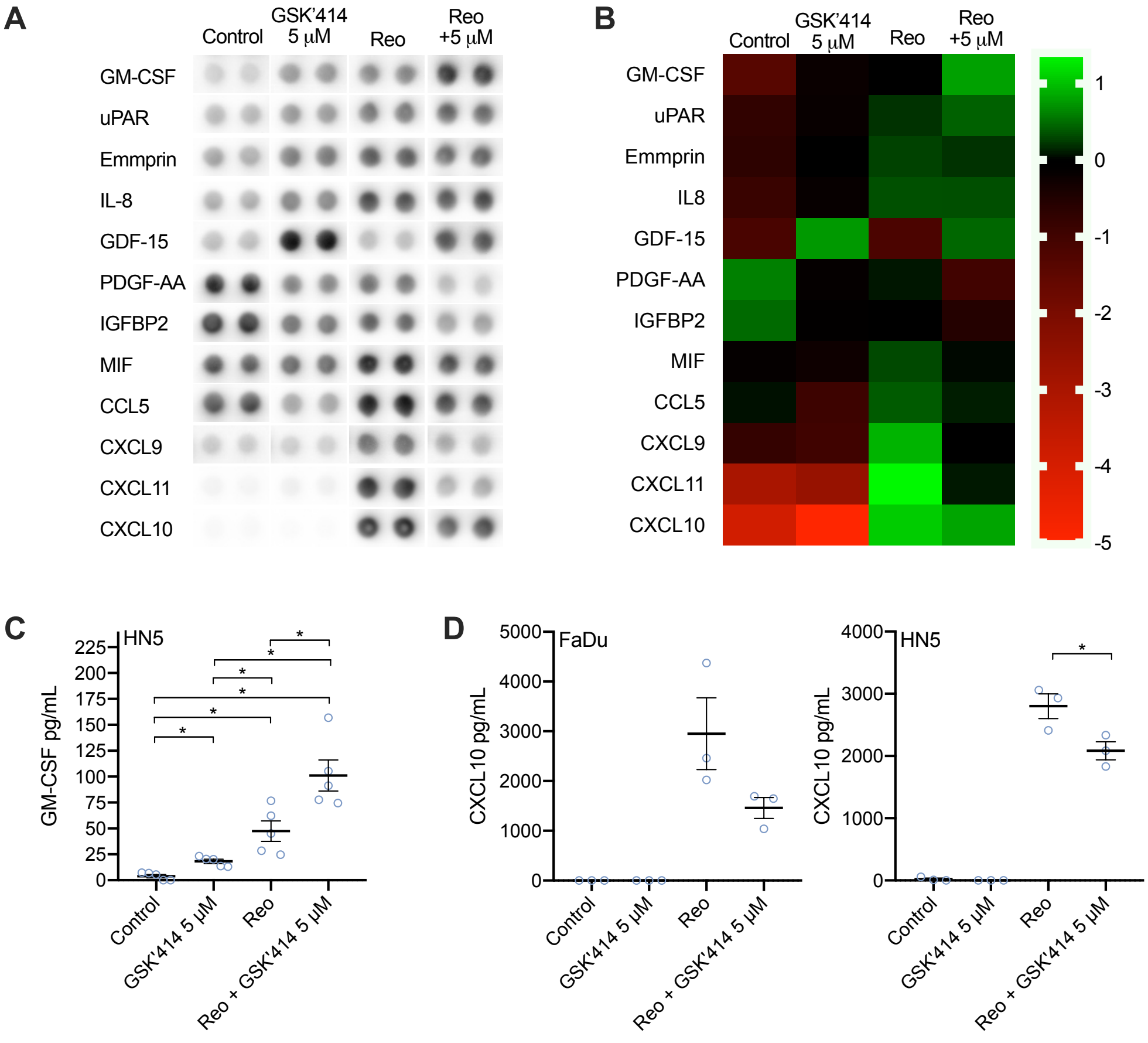
A
Control
GSK'414 5 μM
Reo
Reo +5 μM
GM-CSF
uPAR
Emmprin
IL-8
GDF-15
PDGF-AA
IGFBP2
MIF
CCL5
CXCL9
CXCL11
CXCL10
B
Control
GSK'414 5 μM
Reo
Reo +5 μM
GM-CSF
uPAR
Emmprin
IL8
GDF-15
PDGF-AA
IGFBP2
MIF
CCL5
CXCL9
CXCL11
CXCL10
1
0
-1
-2
-3
-4
-5
C
HN5
GM-CSF pg/mL
225
200
175
150
125
100
75
50
25
0
Control
GSK'414 5 μM
Reo
Reo + GSK'414 5 μM
D
FaDu
CXCL10 pg/mL
5000
4000
3000
2000
1000
0
Control
GSK'414 5 μM
Reo
Reo + GSK'414 5 μM
HN5
CXCL10 pg/mL
4000
3000
2000
1000
0
Control
GSK'414 5 μM
Reo
Reo + GSK'414 5 μM